16–19 September
Milan, Italy 2024

Proof of Concept Magnetic Field Monitoring in Flooded Lead Acid Cells

Scarleth Vasconcelos MSSE
svasconc@villanova.edu

Funded by Consortium for Battery Innovation

PI: Dr. Pritpal Singh
pritpal.singh@villanova.edu

College of Engineering, Villanova University, Villanova, PA 19085

September 18th, 2024

Agenda

1- Introduction

2- Objectives of this Research

3- Methodology

4- Experimental Results

5- Conclusions

Failure Modes in Lead Acid Batteries (LABs)

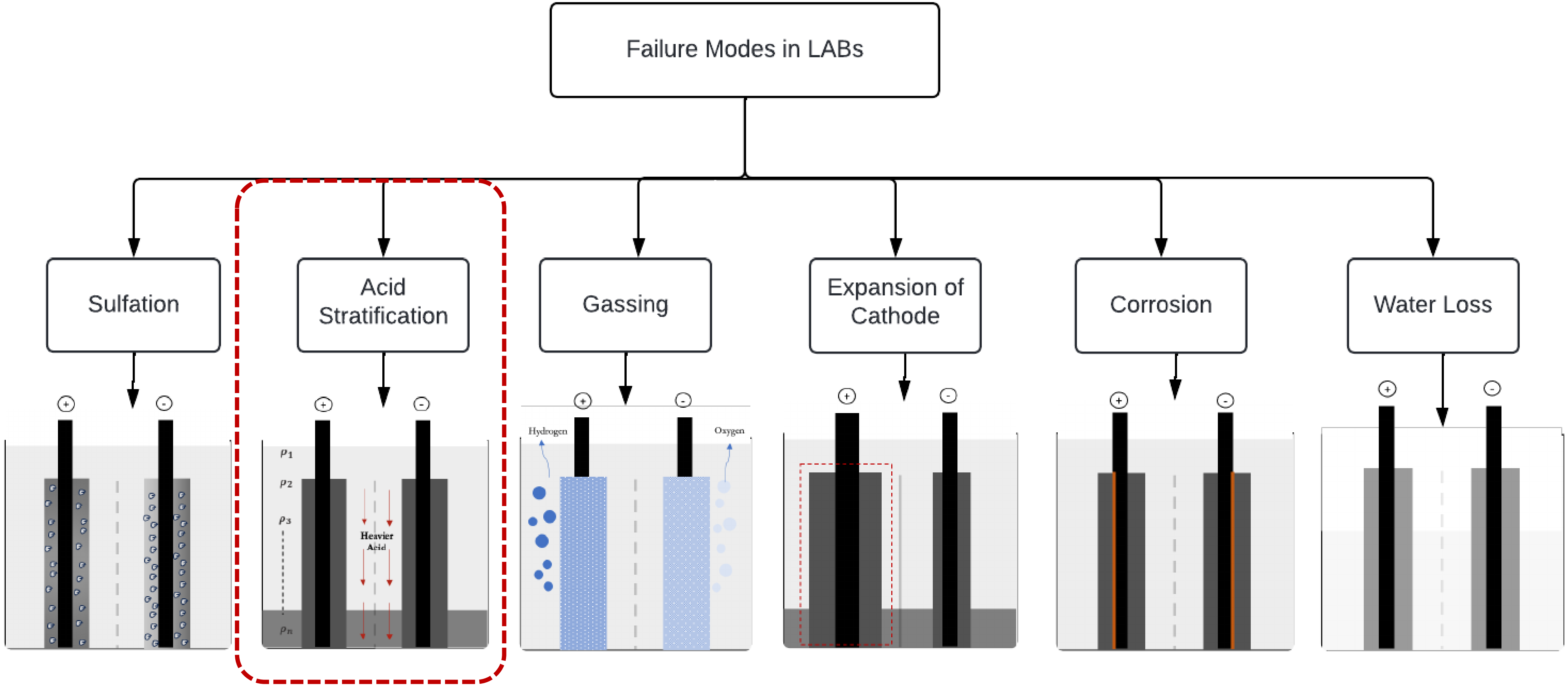

Electrolyte Variations During Cycling

Acid stratification in flooded batteries can develop fast, leading to permanent damage due to inhomogeneous current distribution in the vertical direction of the electrodes.

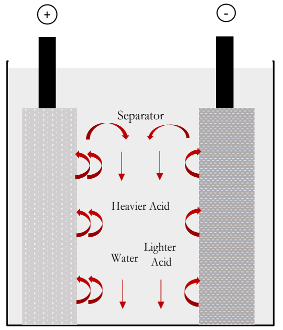

$Pb + PbO_2 + 2H_2SO_4 \rightarrow 2PbSO_4 + 2H_2O$

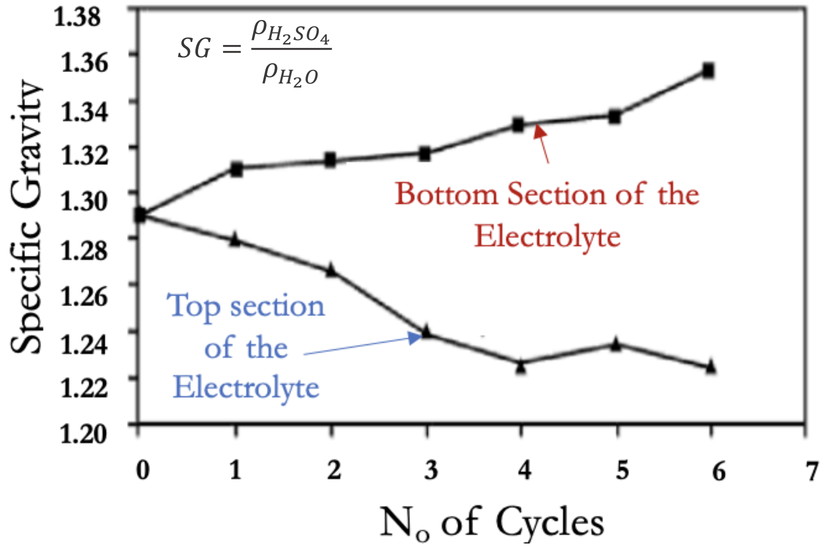

Changes in acid concentration in the top and bottom electrolyte layers on cell cycling

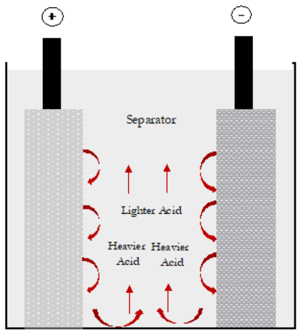

$2PbSO_4 + 2H_2O \rightarrow Pb + PbO_2 + 2H_2SO_4$

SoC	Specific Gravity
100%	1.33
75%	1.37
50%	1.27
25%	1.24
Discharged	1.21

Specific gravity between full charge and discharge cell. Assumes Flooded cell design [3]

Measurements of magnetic susceptibility provide insights about changes in H^+ concentration in the cell.

Research Gaps from Literature Review

Lack of techniques that can accurately and comprehensively assess stratification in LABs at different SoCs.

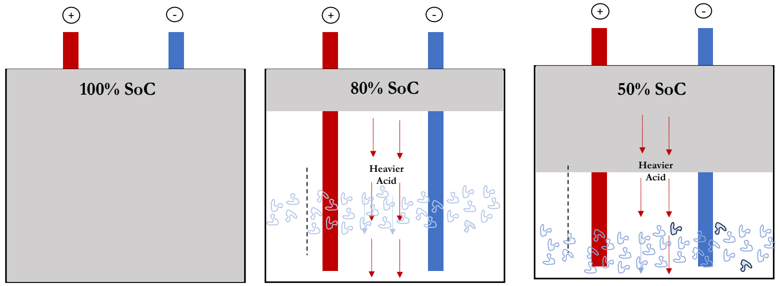

Need for improved sensitivity, accuracy, and validation of methods such as magnetic field imaging, magnetic susceptibility monitoring, and magnetic field probing to predict battery SoH.

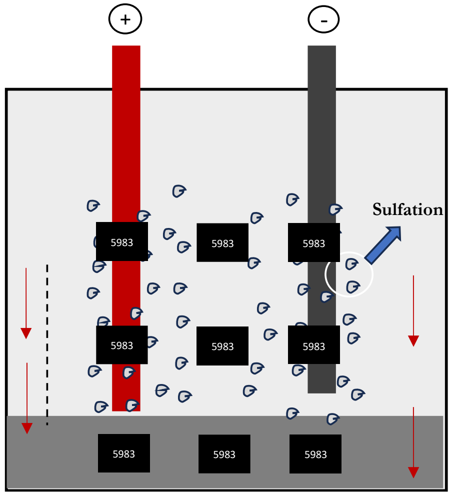

Further research is required for precise SoH estimation in flooded LABs.

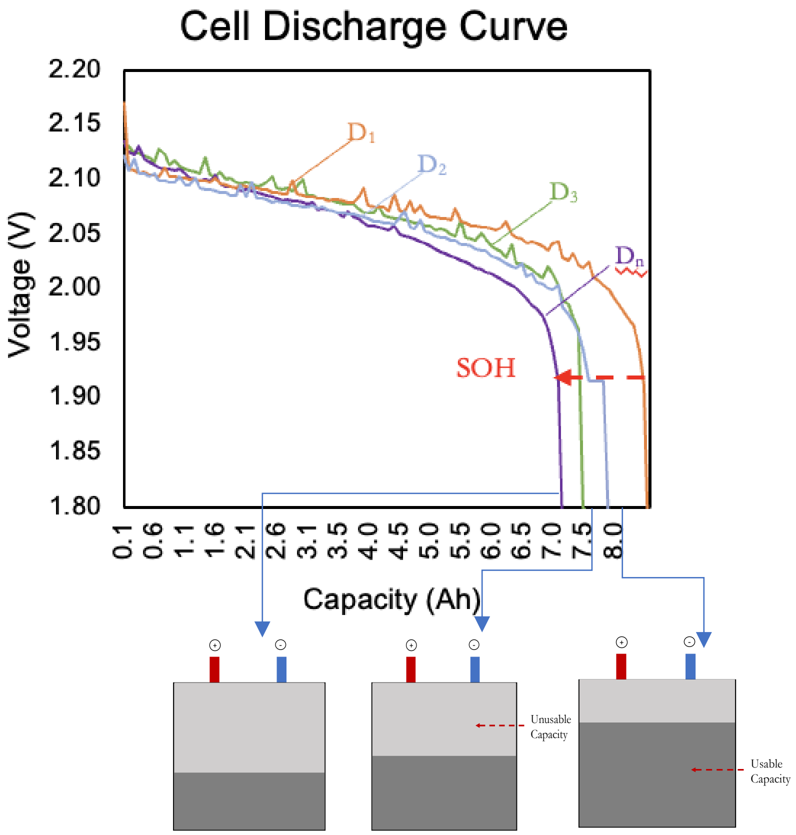

The motivation behind this research is the **need for advanced techniques to detect stratification in flooded lead-acid batteries at different SoCs.**

The general objective is **to develop a real-time battery monitoring system that is non-invasive, non-destructive, and highly accurate for flooded LABs applications**.

The objective of this stage is to **measure the magnetic field response at the electrolyte level in full flooded lead acid cells.**

Magnetic Field Technique Working Principle

Through mutual inductance changes in magnetic field are mapped

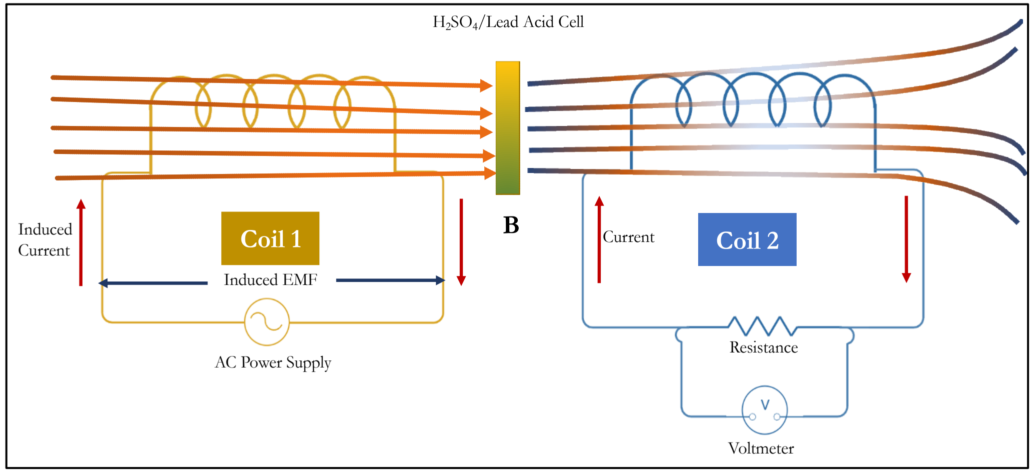

Coupled Coils Setup

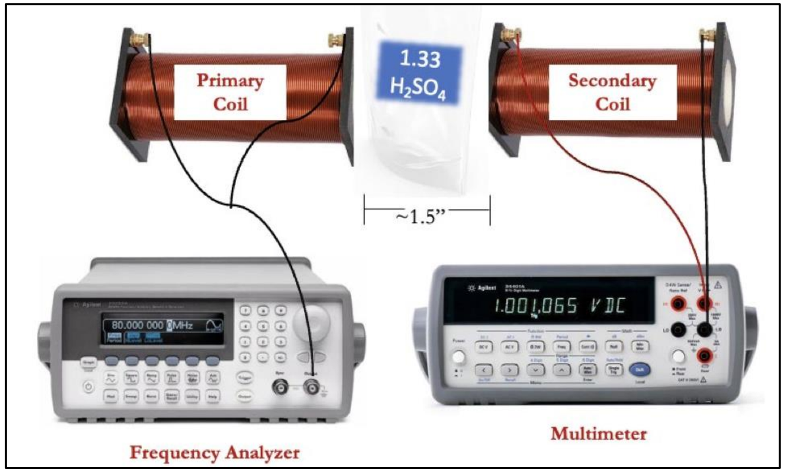

Primary and Secondary Coil Positioning with Electrolyte Solutions

Resonance in magnetic field coupling between two external coupled coils can be used to detect stratification inside the cell.

An AC signal with variable voltage and frequency was applied to the primary coil, and the output voltage across the secondary coil was measured. The measurements were optimized to achieve the largest signal response in the output coil.

Objectives of this Research

Objective 1:

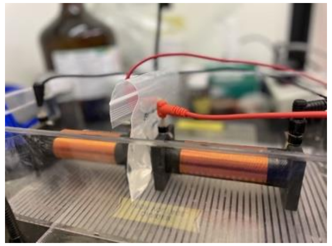

Objective 1.1: Secondary Coil Output Voltage (SCOV) Variations at Individual Electrolytes

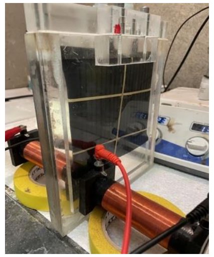

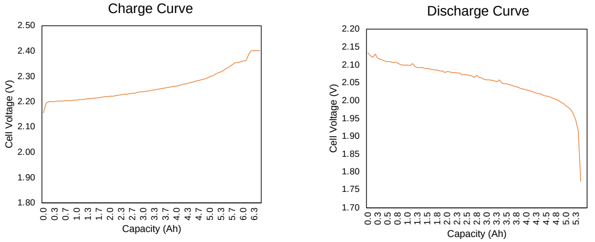

Objective 1.1: Secondary Coil Output Voltage (SCOV) Variations with Coil Separation at Electrolyte Level in a Full Cell during cycling

Objective 2:

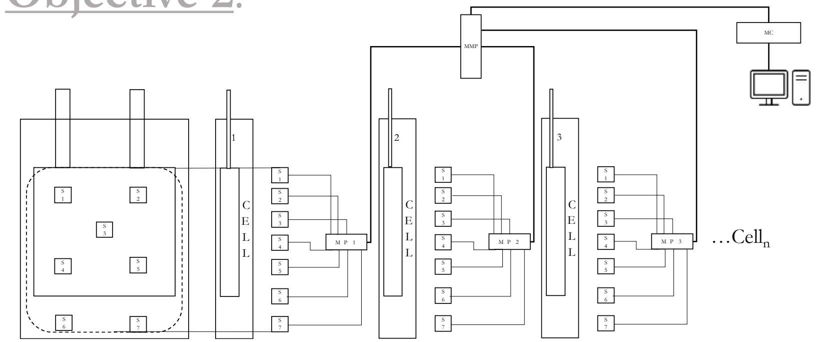

The magnetic field will be mapping using an array of magnetoresistive sensors for 6 cells, 200 cycles

Compare with magnetic imaging scans to identify correlations

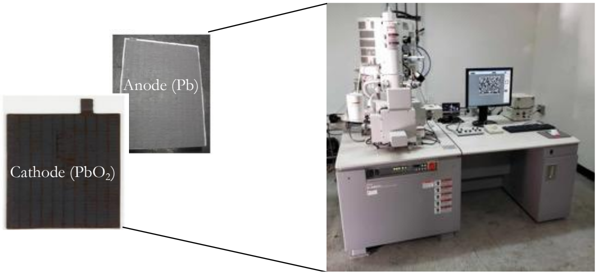

- Map elemental composition of the electrodes
- Perform energy dispersive x-ray analysis

Objective 3:

Simulate the magnetic field mapping of flooded lead acid cells using finite element modeling in the COMSOL Multiphysics environment.

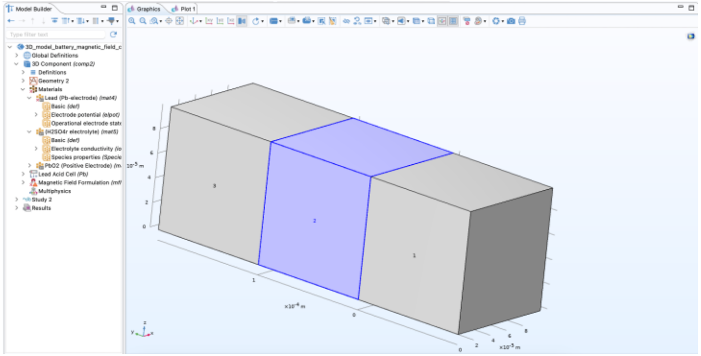

3D Lead Acid Cell Simulation-Adapted from Dr. Parmender Singh Model for Li-ion Electrochemistry.

The simulated results will be compared to the experimental findings obtained from objectives 1 and 2.

Experimental Approach

Prepare Electrolyte at Different Concentrations

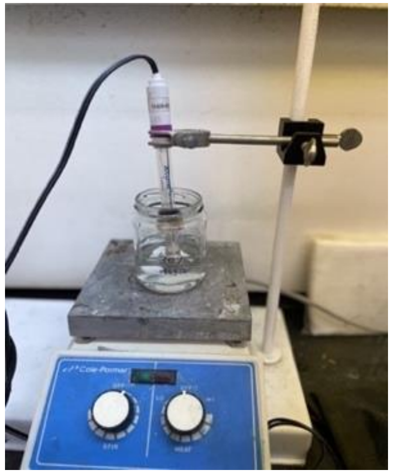

pH Measurement at the Electrolyte Level

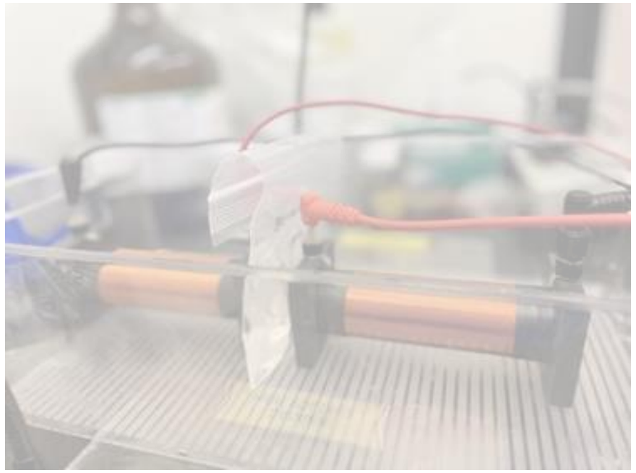

Coupled Coils Measurements at Different Electrolyte Concentrations

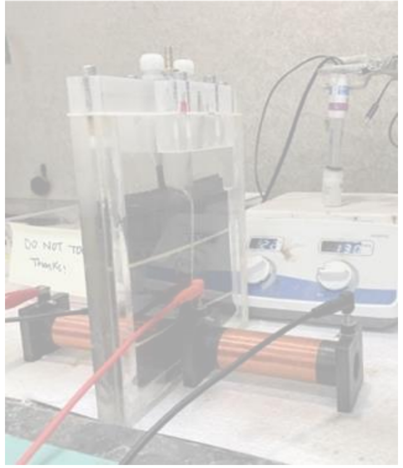

Coupled Coils Measurements at the Cell Lower Electrolyte Level

Preparation of Solutions		
SG (H_2SO_4)	**H_2SO_4 (ml)**	**H_2O (ml)**
1.07	20ml	80ml
1.14	40ml	60ml
1.20	60ml	40ml
1.33	80ml	20ml

Table 1. Preparation of 10%-40% H_2SO_4 Solutions

H_2SO_4 Concentration	**pH Theoretical Value**
1.07	-0.337
1.14	-0.667
1.20	-0.872
1.33	-1.026

Table 2. Theoretical pH for 10%-40% H_2SO_4 Concentrations

Input Data		**Output Data**
Frequency Range (kHz)	**Primary Coil V_{RMS} (V)**	**Secondary Coil V_{RMS} (V)**
10		1.07 H_2SO4
20		
30	3.535	1.14 H_2SO4
40		
50		1.20 H_2SO4
60		
70		1.33 H_2SO4

Ranges of Frequency and Voltage Input at Different H_2SO_4 Concentrations

pH Measurement Results

The pH was measured to represent changes in concentration at the electrolyte during cell's cycling.

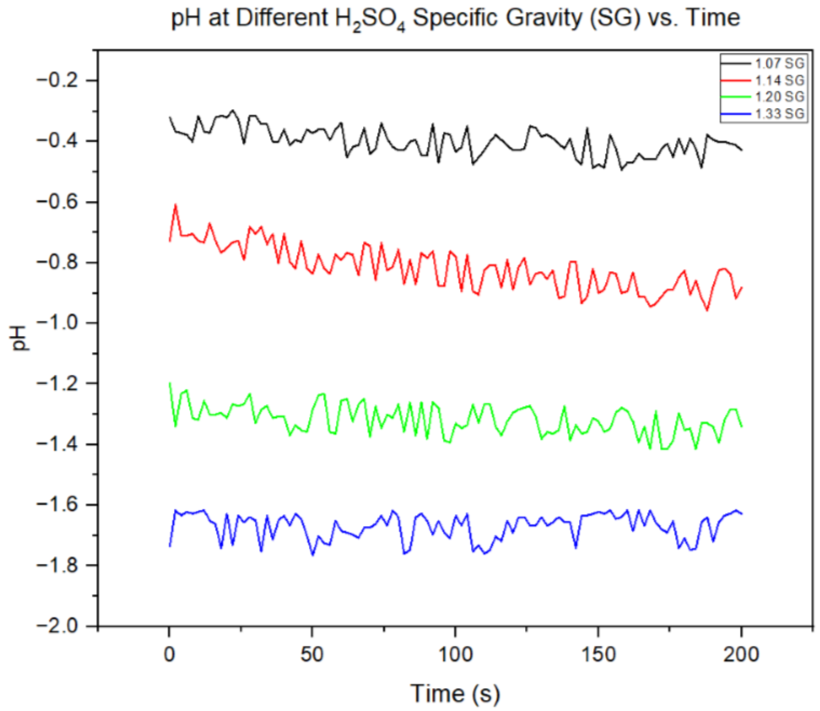

pH Measurements for 1.07-1.33 H_2SO_4 Concentrations

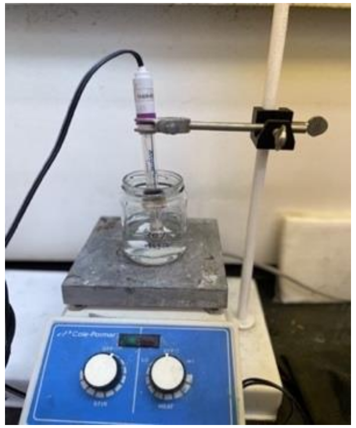

pH Measurement for Different H_2SO_4 Concentrations

H_2SO_4	pH	Stdv
1.07	-0.40	0.05
1.14	-0.82	0.07
1.20	-1.32	0.05
1.33	-1.67	0.04

pH Measurements for 1.07-1.33 H_2SO_4 Concentrations

As the Sulfuric acid concentration increases the pH decreases due to donation of H^+ to water.

At the cell level, during discharge sulfuric acid is consumed and water is produced.

Experimental Approach

Prepare Electrolyte at Different Concentrations

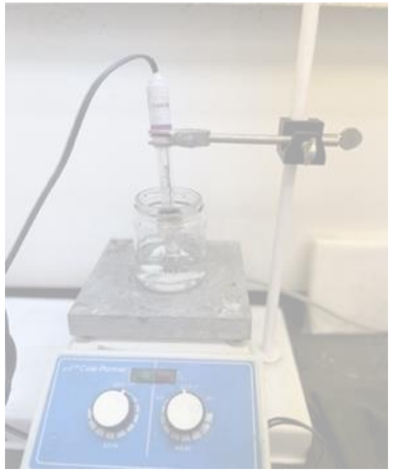

pH Measurement at the Electrolyte Level

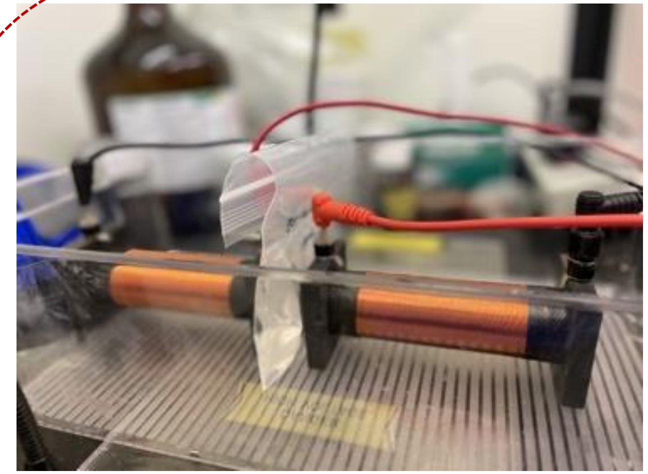

Coupled Coils Measurements at Different Electrolyte Concentrations

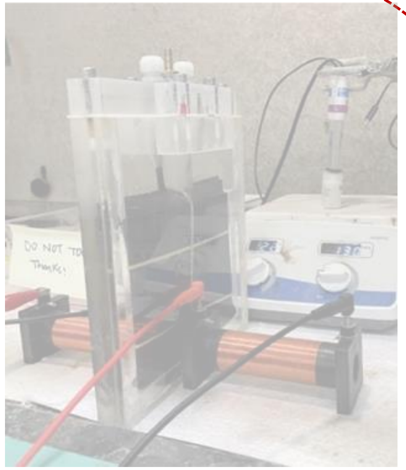

Coupled Coils Measurements at the Cell Lower Electrolyte Level

Preparation of Solutions		
(H_2SO_4)	H_2SO_4 (ml)	H_2O (ml)
1.07	20ml	80ml
1.14	40ml	60ml
1.20	60ml	40ml
1.33	80ml	20ml

Preparation of 10%-40% H_2SO_4 Solutions

H_2SO_4 Concentration	pH Theoretical Value
1.07	-0.337
1.14	-0.667
1.20	-0.872
1.33	-1.026

Theoretical pH for 10%-40% H_2SO_4 Concentrations

Input Data		Output Data
Frequency Range (kHz)	Primary Coil V_{RMS} (V)	Secondary Coil V_{RMS} (V)
10		1.07 H_2SO_4
20		
30		1.14 H_2SO_4
40	0.5-3.5	
50		1.20 H_2SO_4
60		
70		1.33 H_2SO_4

Ranges of Frequency and Voltage Input at Different H_2SO_4 Concentrations

Characterization of Frequency and Amplitude Input Values

VILLANOVA UNIVERSITY

-Frequencies: 10-70kHz
 (5kHz interval)
-Amplitude Voltage: 0.5-3.5V
 (0.5V steps)
-H_2SO_4 concentrations: 1.07-1.33
 (1.6-1.33 SG)

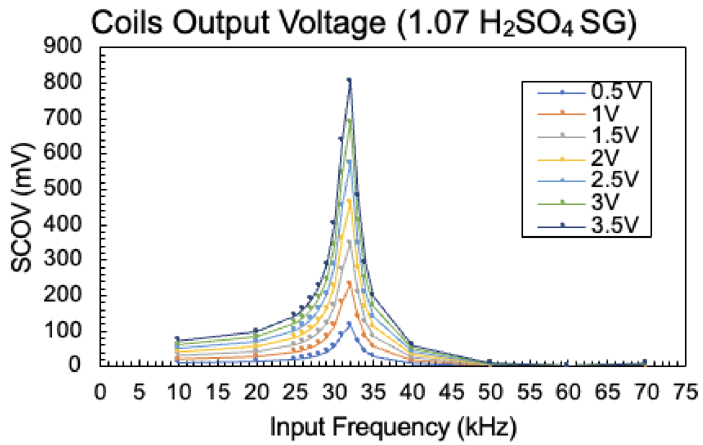

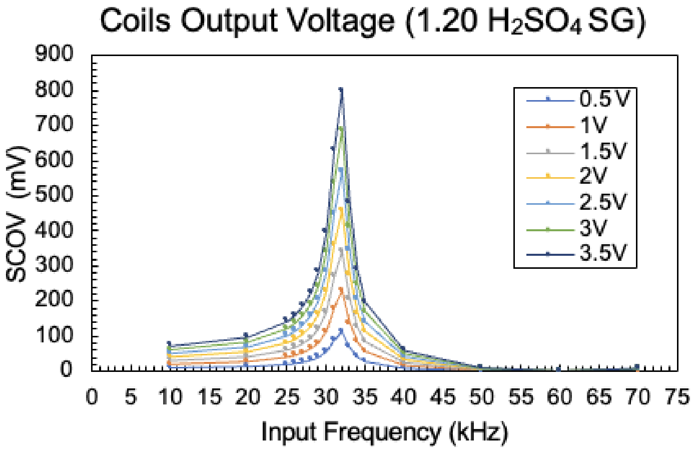

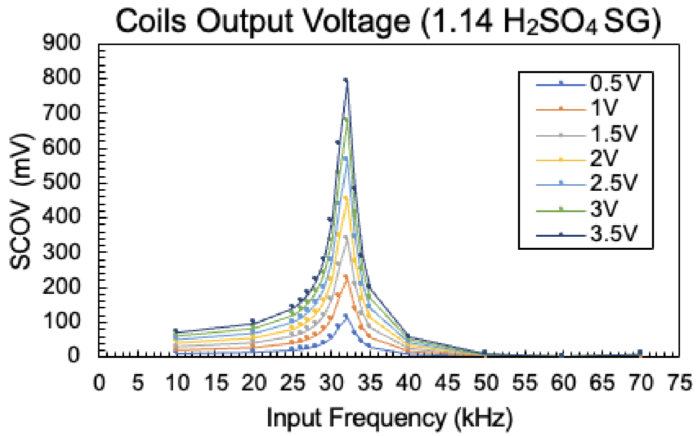

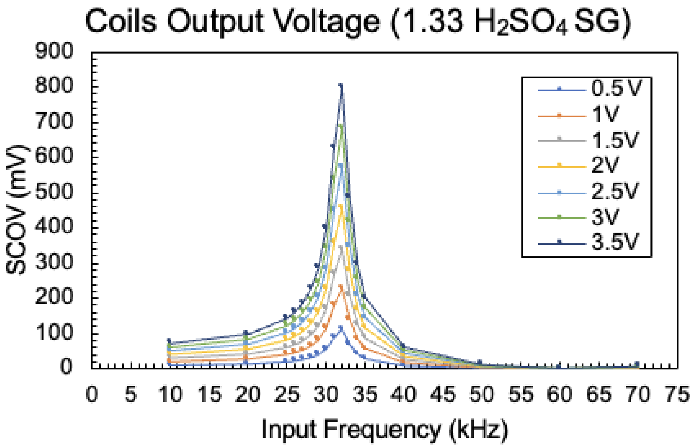

SCOV Variation with Coil Separation

-Frequency Used: 10-70kHz (5kHz interval;1kHz interval 25-35kHz)
-Input Amplitude Voltage: 0.5-3.5V (0.5V interval)

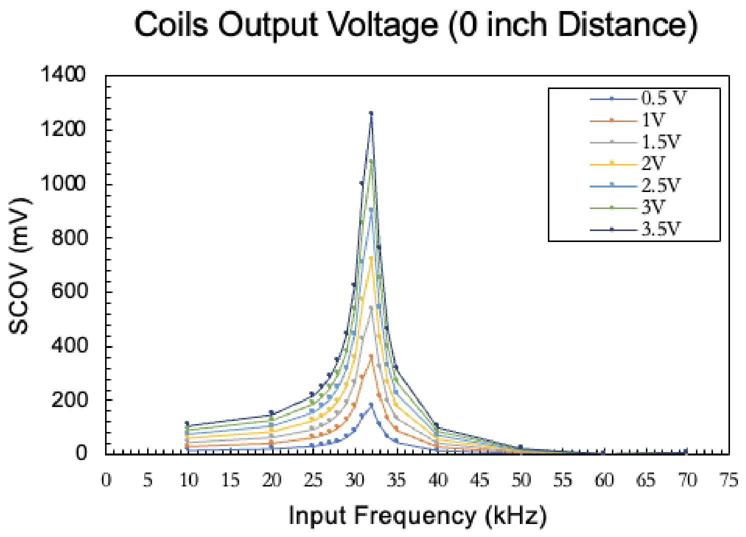

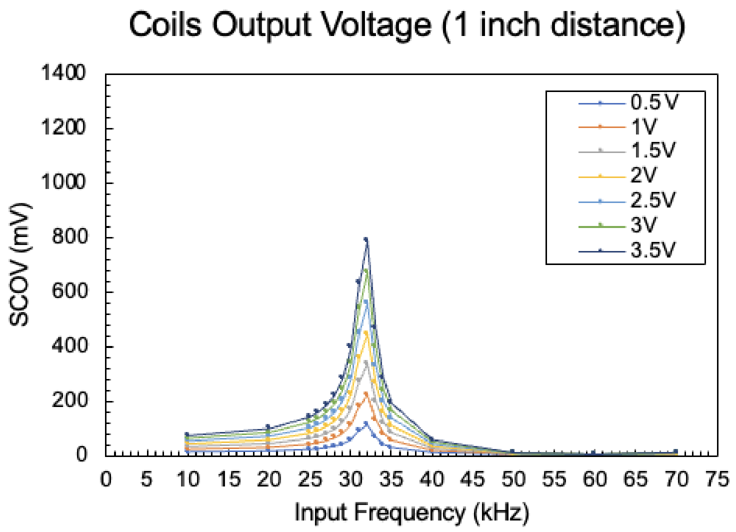

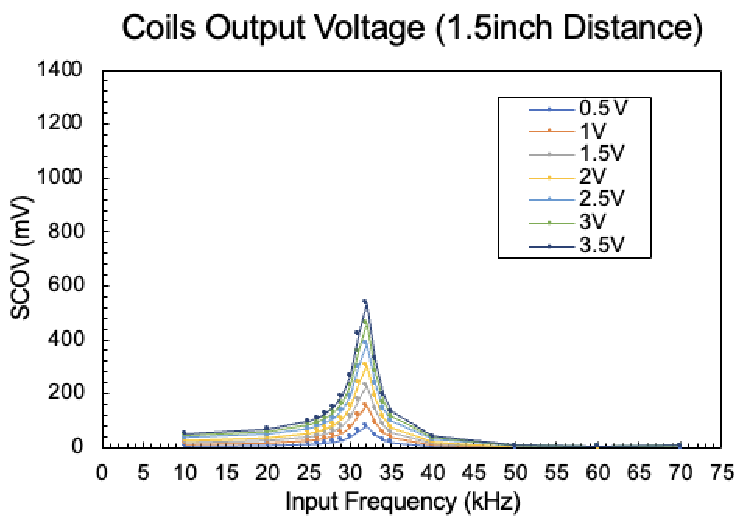

Note changes in output voltage as distance between coils increase

SCOV at Different H_2SO_4 Concentrations

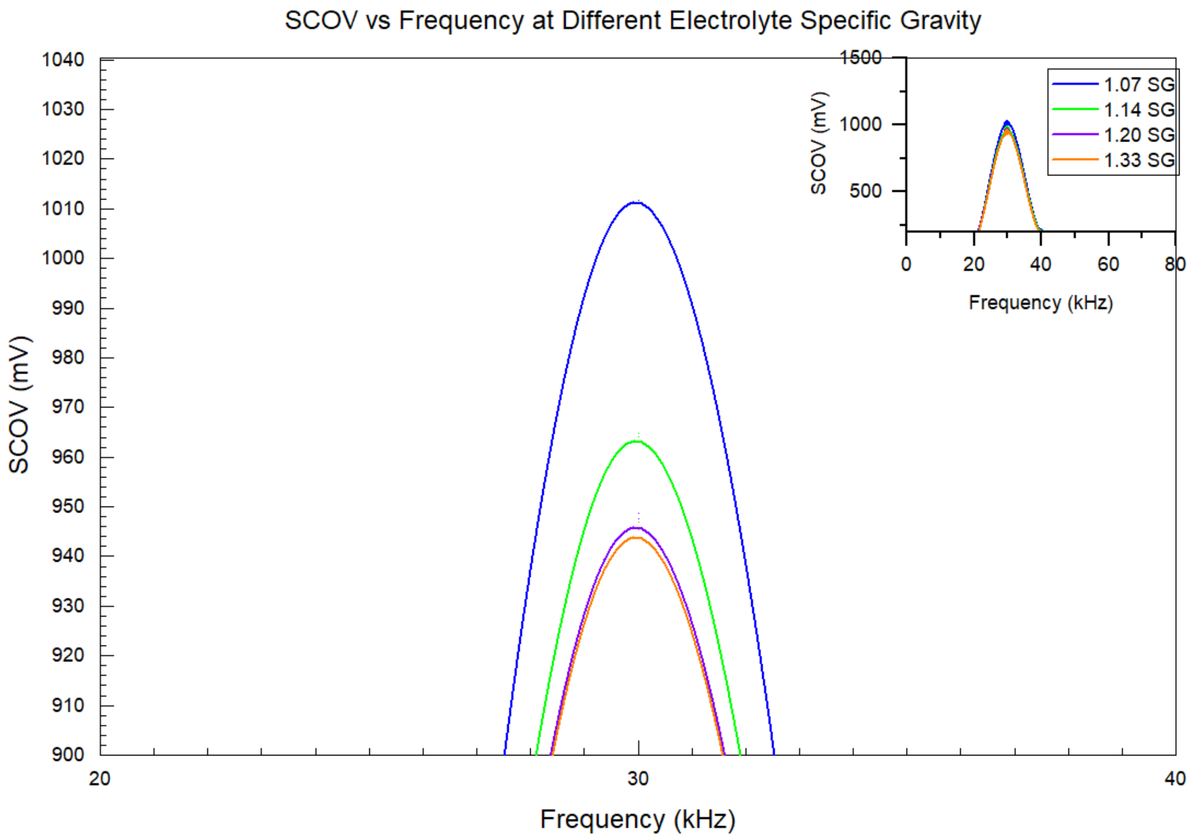

Coupled Coils Measurements in Sulfuric Acid

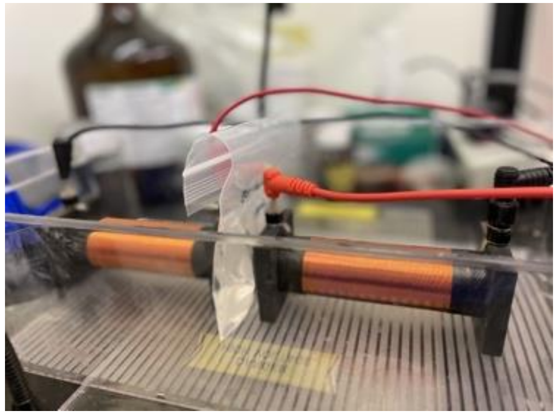

Coupled Coils Measurements at Different Electrolyte Concentrations

Frequency (kHz)	1.07 H_2SO_4	1.14 H_2SO_4	1.20 H_2SO_4	1.33 H_2SO_4
10	77.0	75.8	76.2	75.7
20	134.5	130.9	130.8	130.3
30	**1011.3**	**964.0**	**947.3**	**945.2**
40	198.0	188.4	187.0	187.4
50	102.3	96.0	94.7	95.2
60	74.1	69.1	69.0	68.4
70	60.4	56.0	55.0	55.3

Average Results of Output Voltage (mV)

The optimal AC input frequency maximizes the induced magnetic field response

Experimental Approach

Introduction | Objectives | **Methodology**

Prepare Electrolyte at Different Concentrations

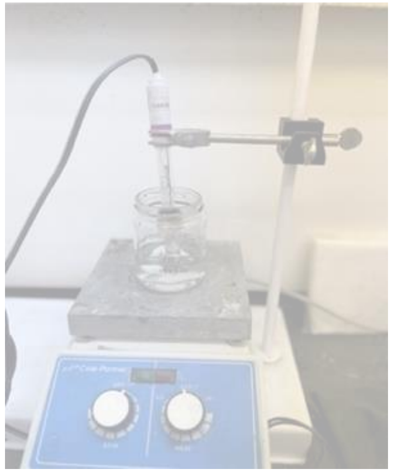

pH Measurement at the Electrolyte Level

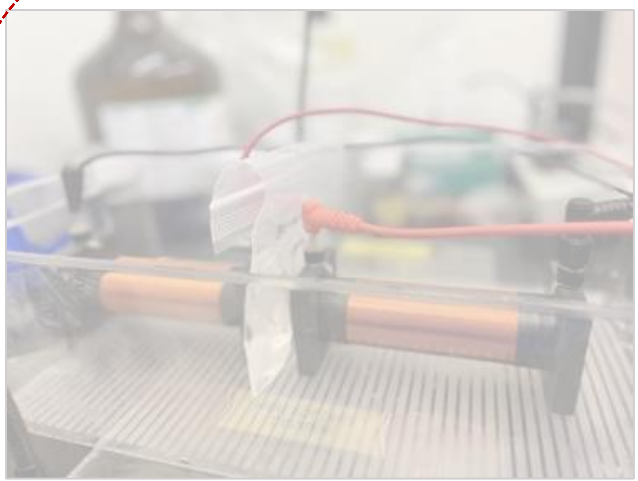

Coupled Coils Measurements at Different Electrolyte Concentrations

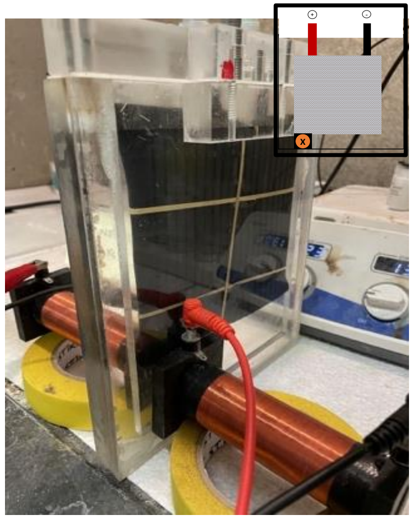

Coupled Coils Measurements at the Cell Lower Electrolyte Level

Preparation of Solutions		
(H_2SO_4)	H_2SO_4 (ml)	H_2O (ml)
1.07	25ml	75ml
1.14	50ml	50ml
1.20	75ml	25ml
1.33	100ml	0ml

Preparation of 10%-40% H_2SO_4 Solutions

H_2SO_4 Concentration	pH Theoretical Value
1.07	-0.337
1.14	-0.667
1.20	-0.872
1.33	-1.026

Theoretical pH for 10%-40% H_2SO_4 Concentrations

Input Data		Output Data
Frequency Range (kHz)	Primary Coil V_{RMS} (V)	Secondary Coil V_{RMS} (V)
30-35	3.535	1.33H_2SO_4

Ranges of Frequency and Voltage Input at Different H_2SO_4 Concentrations

SCOV During Discharge (Lower-Left Section of Electrolyte)

The SCOV gradually increases as the electrolyte concentration decreases

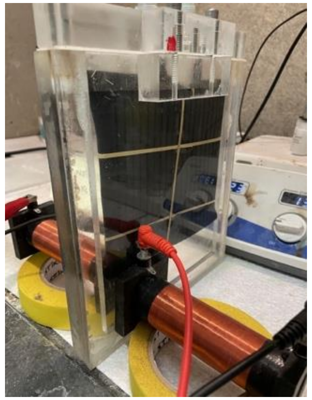

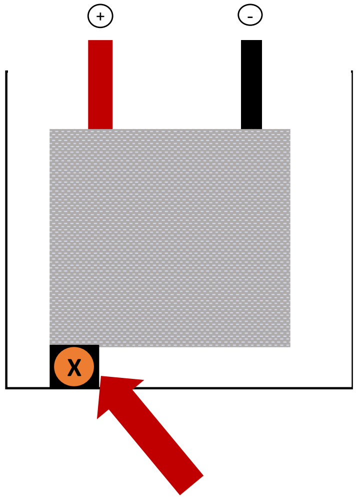

Primary and Secondary Coils Positioned at the Left Lower Section in the Cell-Electrolyte Only

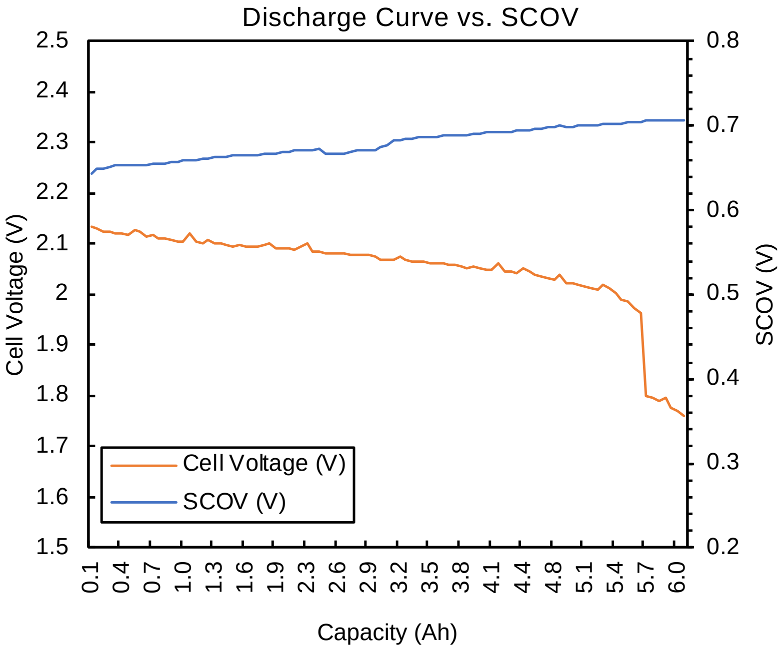

Results from Experimental Approach of Output Voltage at 33kHz Input Voltage During Discharge

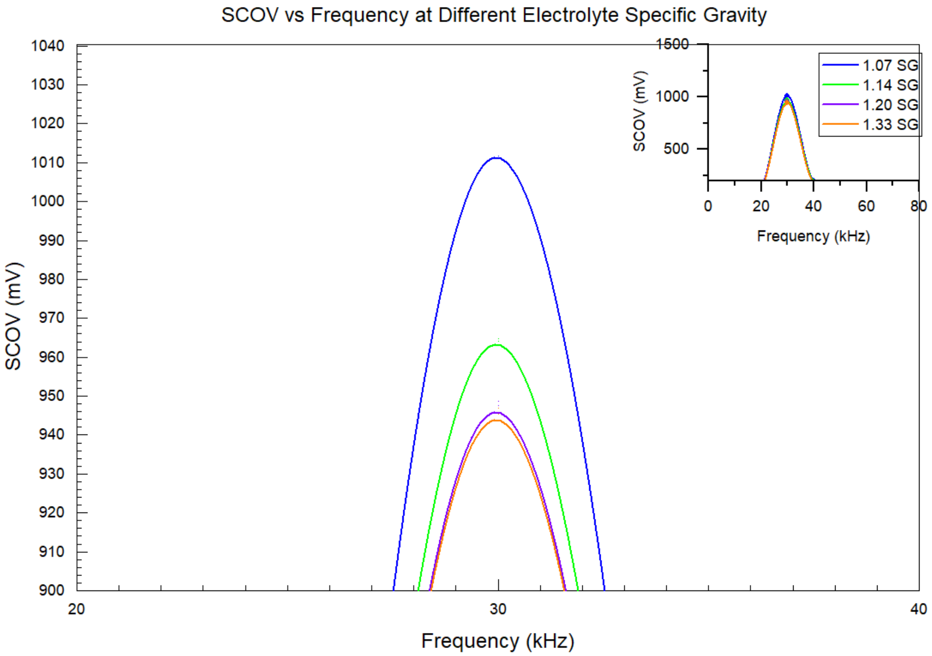

Results from Experimental Approach of Output Voltage at 30kHz Frequency

SCOV During Charge (Lower-Left Section of Electrolyte)

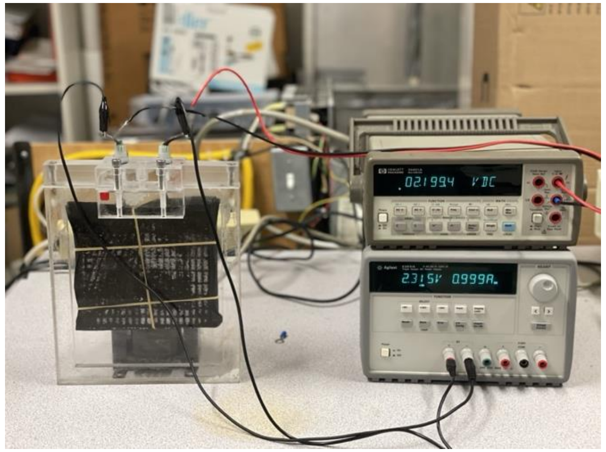

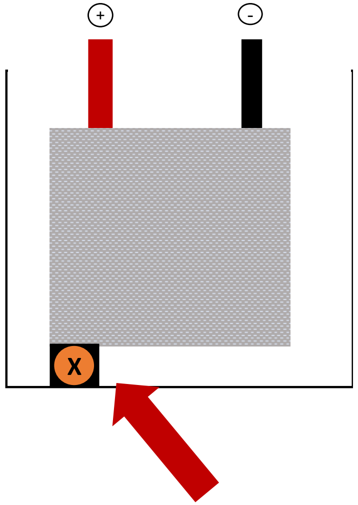

Primary and Secondary Coils Positioned at the Left Lower Section in the Cell-Electrolyte Only

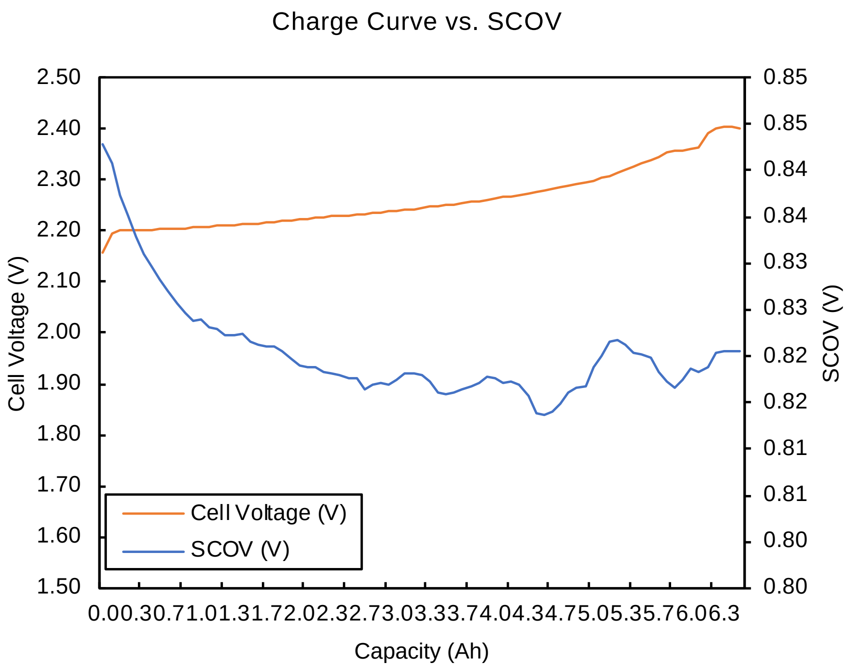

Results from Experimental Approach of Output Voltage at 33kHz Input Voltage During Charge

Takeaways from Preliminary Experimental Results

VILLANOVA UNIVERSITY

pH Electrolyte Measurements

- pH measurements were conducted at various sulfuric acid concentrations ranging from 1.07 to 1.33 specific gravity.
- The data obtained consistently and reproducibly showed a measurable relationship between these concentrations and the corresponding pH levels, particularly at very low pH values.

Secondary Coil Output Voltage (SCOV) at Lower Electrolyte Level

- The optimal AC input frequency that maximizes the induced magnetic field response lies in the range of 30kHz-33kHz, depending on the physical properties of the magnetic field inductors (air core solenoid coils).
- A clear correlation between the output voltage resulting from the interaction of the induced magnetic field and changes in the electrolyte concentration was observed.
- If we increase the input voltage at the primary coil then the magnetic field excitation increases and the voltage at the secondary coil also correspondingly increases.

Takeaways from Preliminary Experimental Results

Secondary Coil Output Voltage (SCOV) at Electrolyte Level in a Full Cell

- The magnetic field decreases during charging and increases during discharge
- The H+ proton concentration in the electrolyte and the SCOV both vary with the specific gravity during battery cycling

These findings provide a foundation for the development of an efficient and effective battery monitoring system, that has the potential to significantly improve the reliability and lifespan of flooded LABs.

Objectives of this Research

Objective 1:

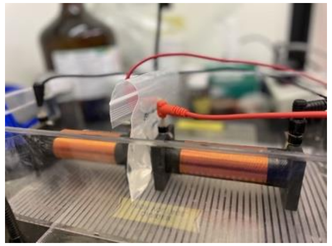

Objective 1.2: Secondary Coil Output Voltage (SCOV) Variations at individual Electrolytes

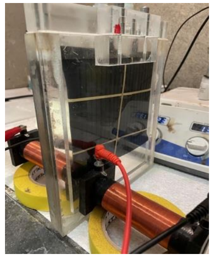

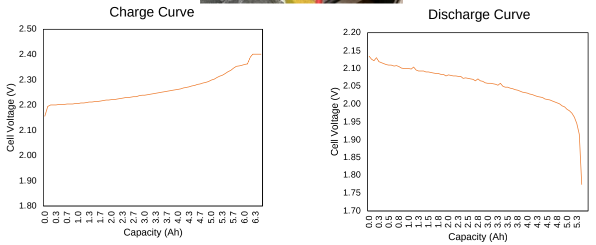

Objective 1.3: Secondary Coil Output Voltage (SCOV) Variations with Coil Separation at Electrolyte Level in a Full Cell during cycling

Objective 2:

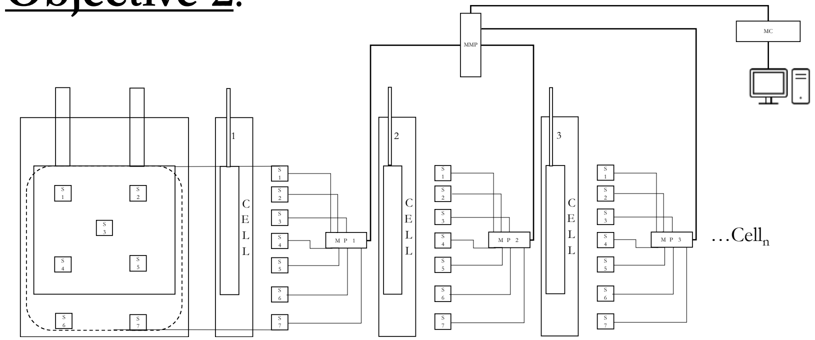

The magnetic field will be mapping using an array of magnetoresistive sensors for 6 cells, 200 cycles

Compare with magnetic imaging scans to identify correlations

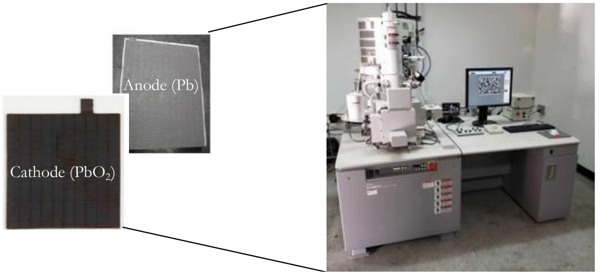

- Map elemental composition of the electrodes
- Perform energy dispersive x-ray analysis

Objective 3:

Simulate the magnetic field mapping of flooded lead acid cells using finite element modeling in the COMSOL Multiphysics environment.

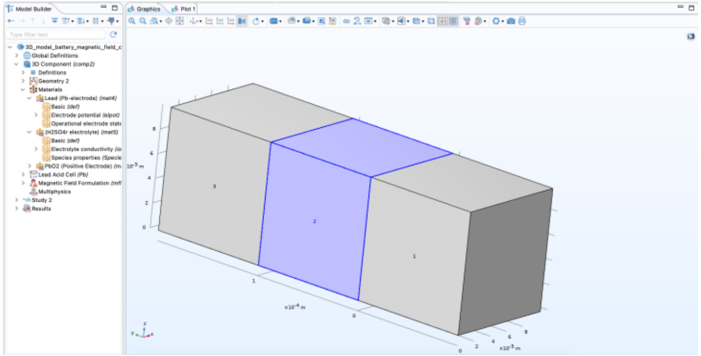

3D Lead Acid Cell Simulation-Adapted from Dr. Parmender Singh Model for Li-ion Electrochemistry.

The simulated results will be compared to the experimental findings obtained from objectives 1 and 2.

O2: Proof of Concept for Magnetoresistive Sensors

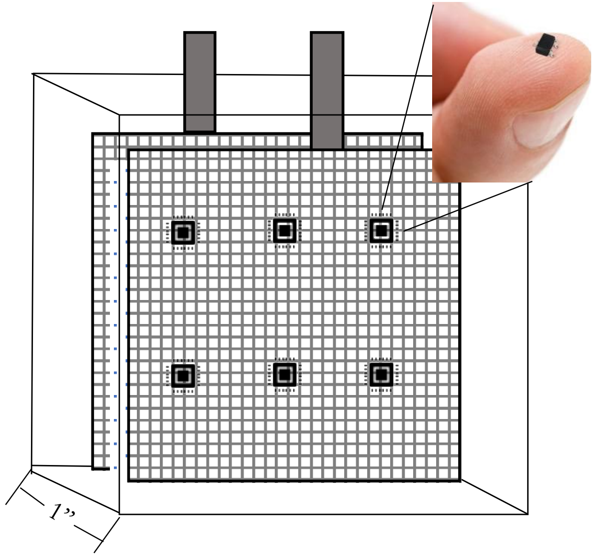

$$B_m = \frac{4X10{-}7\frac{Tm}{A}(1A)}{2\pi(0.0127m)}$$

$B_m = 1.5x10^{-5}T$ or 0.15 G

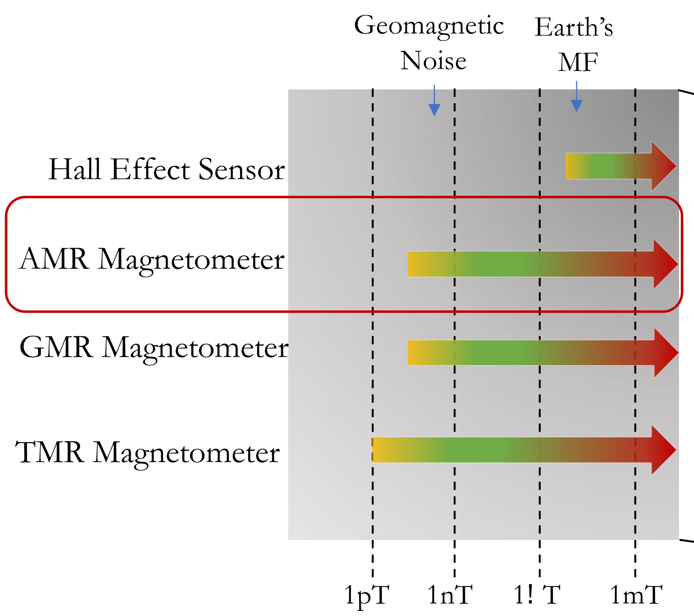

Fig 24. Estimate of sensitivity of different magnetic sensors.

Anisotropic Magnetoresistance (AMR)

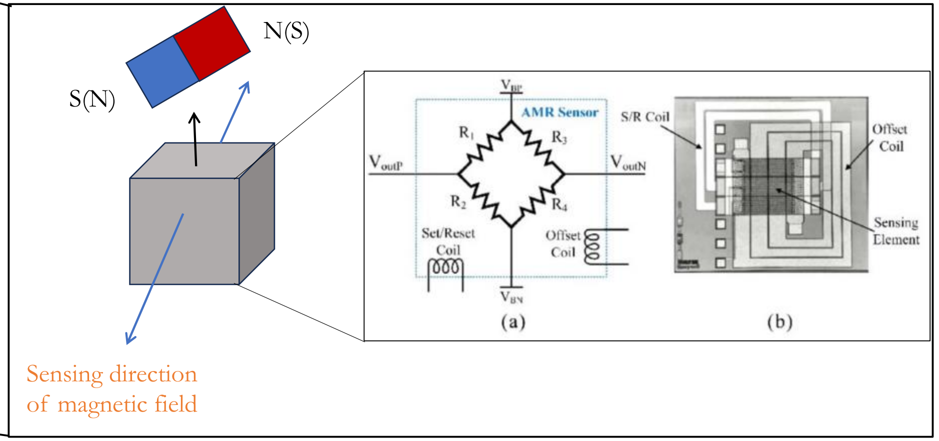

Use of permalloy, an alloy of nickel and iron whose resistance changes proportionally when presented with a magnetic field. Via analog circuitry, the resistance is then converted to a voltage. The voltage generated is directly proportional to the original current.

Experimental Setup with Sensors

Extract Aged and Fresh Cells

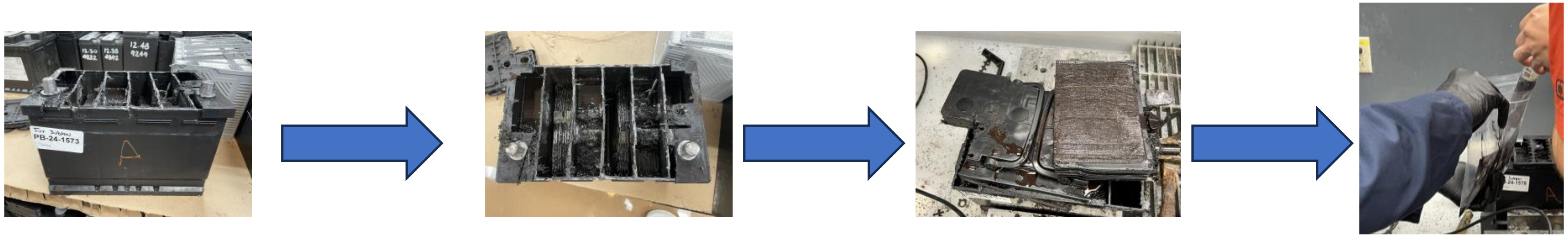

3 Cells-60 Cycles and 3 Cells-Pristine | Specific Gravities: 1.07-1.30

Place Magnetoresistors at the Cell's Electrolyte Level

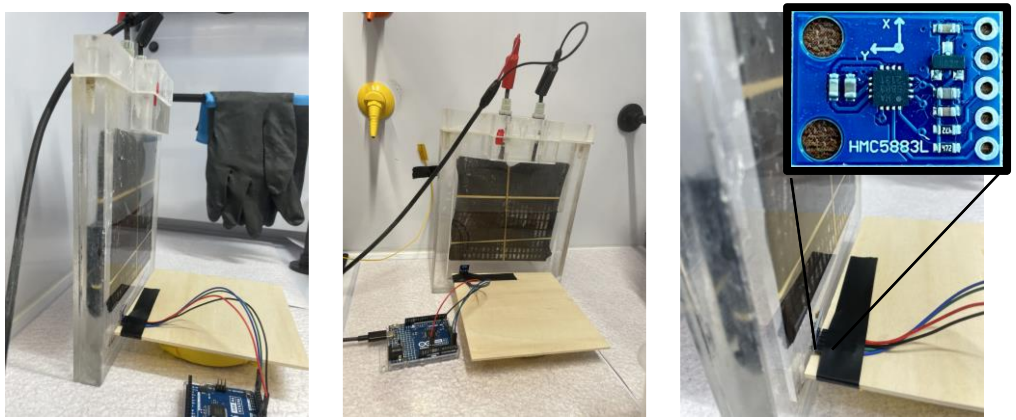

Objectives of this Research

Objective 1:

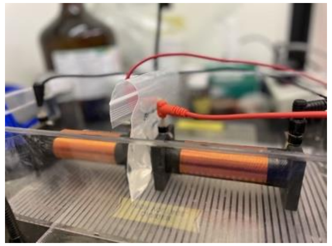

Objective 1.2: Secondary Coil Output Voltage (SCOV) Variations at individual Electrolytes

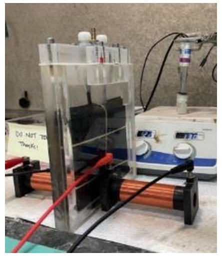

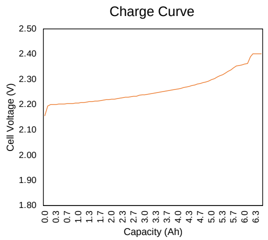

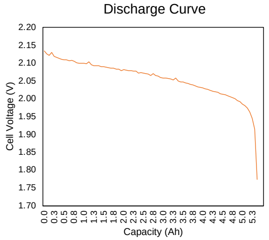

Objective 1.3: Secondary Coil Output Voltage (SCOV) Variations with Coil Separation at Electrolyte Level in a Full Cell during cycling

Objective 2:

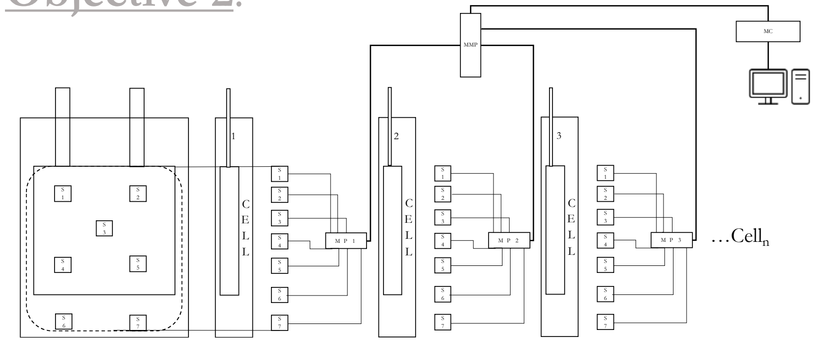

The magnetic field will be mapping using an array of magnetoresistive sensors for 6 cells, 200 times

Compare with magnetic imaging scans to identify correlations

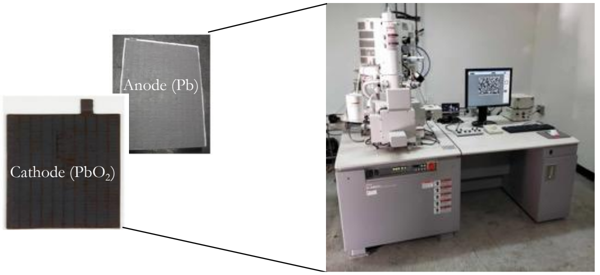

- Map elemental composition of the electrodes
- Perform energy dispersive x-ray analysis

Objective 3:

Simulate the magnetic field mapping of flooded lead acid cells using finite element modeling in the COMSOL Multiphysics environment.

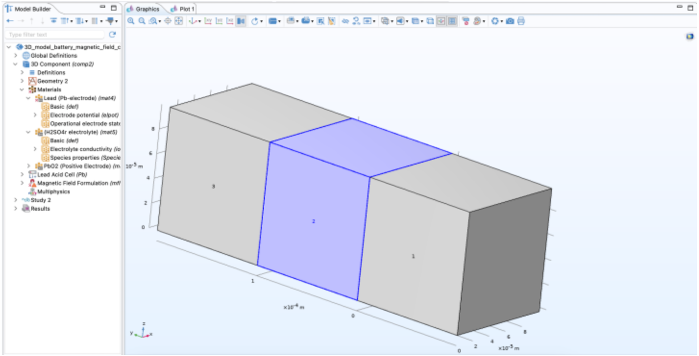

3D Lead Acid Cell Simulation-Adapted from Dr. Parmender Singh Model for Li-ion Electrochemistry.

The simulated results will be compared to the experimental findings obtained from objectives 1 and 2.

Acknowledgements

Corporate Supporters:

Dr. Matthew Raiford, *Consortium of Battery Innovation (CBI)*
Dr. Subhas Chalasani, Michael Evans, William Kunsman and Brian Zimmerman, *East Penn Manufacturing Corporation*

Advising Committee:

<u>Villanova University:</u>

Dr. Ross Lee, *Sustainable Engineering (Advisor)*
Dr. Pritpal Singh, *Electrical and Computer Engineering (Co-advisor)*

Thank You!

Scan Me

Let's Connect

svasconc@villanova.edu

References

[1] S. Jiang and Z. Song, "A review on the state of health estimation methods of lead-acid batteries," *J. Power Sources*, vol. 517, p. 230710, Jan. 2022, doi: 10.1016/j.jpowsour.2021.230710.

[2] D. Linden and T. B. Reddy, Eds., *Handbook of batteries*, 3. ed. in McGraw-Hill handbooks. New York, NY: McGraw-Hill, 2002.

[3] U. Koehler, "Chapter 2 - General Overview of Non-Lithium Battery Systems and their Safety Issues," in *Electrochemical Power Sources: Fundamentals, Systems, and Applications*, J. Garche and K. Brandt, Eds., Elsevier, 2019, pp. 21–46. doi: https://doi.org/10.1016/B978-0-444-63777-2.00002-5.

[4] P.-H. Huang, J.-K. Kuo, and C.-Y. Huang, "A new application of the UltraBattery to hybrid fuel cell vehicles," *Int. J. Energy Res.*, vol. 40, p. n/a-n/a, Oct. 2015, doi: 10.1002/er.3426.

[5]"Fig. 6 Basic chemical reactions in lead-acid batteries," ResearchGate. Accessed: Aug. 21, 2023. [Online]. Available: https://www.researchgate.net/figure/Basic-chemical-reactions-in-lead-acid-batteries_fig3_277716204

[6]J. Lach, K. Wróbel, J. Wróbel, P. Podsadni, and A. Czerwiński, "Applications of carbon in lead-acid batteries: a review," *J. Solid State Electrochem.*, vol. 23, no. 3, pp. 693–705, Mar. 2019, doi: 10.1007/s10008-018-04174-5.

[7] P. Singh, "Energy Storage Systems for Electric Vehicles," Jan. 2019.

[8] D. Pavlov, *Lead-Acid Batteries: Science and Technology: A Handbook of Lead-Acid Battery Technology and Its Influence on the Product*. Elsevier, 2017.

[9] D. Linden and T. B. Reddy, Eds., *Handbook of batteries*, 3rd ed. in McGraw-Hill handbooks. New York: McGraw-Hill, 2002.

[10] *Energy Storage*. Accessed: Apr. 29, 2024. [Online]. Available: https://link.springer.com/book/10.1007/978-3-319-21239-5

[11] S. Jiang and Z. Song, "A review on the state of health estimation methods of lead-acid batteries," *J. Power Sources*, vol. 517, p. 230710, Jan. 2022, doi: 10.1016/j.jpowsour.2021.230710.

[12] "Consortium for Battery Innovation | » Lead battery market data." Accessed: Feb. 07, 2024. [Online]. Available: https://batteryinnovation.org/resources/lead-battery-market-data/

[13] I. Mexis and G. Todeschini, "Battery Energy Storage Systems in the United Kingdom: A Review of Current State-of-the-Art and Future Applications," *Energies*, vol. 13, no. 14, Art. no. 14, Jan. 2020, doi: 10.3390/en13143616.

[14] J. Yang, C. Hu, H. Wang, K. Yang, J. B. Liu, and H. Yan, "Review on the research of failure modes and mechanism for lead–acid batteries," *Int. J. Energy Res.*, vol. 41, no. 3, pp. 336–352, 2017, doi: 10.1002/er.3613.

[15] Y. Zhang *et al.*, "Advances and challenges in improvement of the electrochemical performance for lead-acid batteries: A comprehensive review," *J. Power Sources*, vol. 520, p. 230800, Feb. 2022, doi: 10.1016/j.jpowsour.2021.230800.

[16] M. Mohsin, A. Picot, and P. Maussion, "A new lead-acid battery state-of-health evaluation method using electrochemical impedance spectroscopy for second life in rural electrification systems," *J. Energy Storage*, vol. 52, p. 104647, Aug. 2022, doi: 10.1016/j.est.2022.104647.

[17] D. Schulte, D. U. Sauer, E. Ebner, A. Börger, S. Gose, and H. Wenzl, "'Stratifiability index' – A quantitative assessment of acid stratification in flooded lead acid batteries," *J. Power Sources*, vol. 269, pp. 704–715, Dec. 2014, doi: 10.1016/j.jpowsour.2014.06.155.

References

[18] “Coulomb Efficiency - an overview | ScienceDirect Topics.” Accessed: May 07, 2024. [Online]. Available: https://www.sciencedirect.com/topics/engineering/coulomb-efficiency

[19] J. Garche, E. Karden, P. T. Moseley, and D. A. J. Rand, *Lead-Acid Batteries for Future Automobiles*. Elsevier, 2017.

[20] T. W. Ellis and J. A. MONTENEGRO, “Magnetic separation of electrochemical cell materials,” WO2013148809A1, Oct. 03, 2013 Accessed: May 06, 2024. [Online]. Available: https://patents.google.com/patent/WO2013148809A1/nl

[21] M. Babaei, I. C. Jones, K. Dayal, and M. S. Mauter, “Computing the Diamagnetic Susceptibility and Diamagnetic Anisotropy of Membrane Proteins from Structural Subunits,” *J. Chem. Theory Comput.*, vol. 13, no. 6, pp. 2945–2953, Jun. 2017, doi: 10.1021/acs.jctc.6b01251.

[22] H. T. Harrison, G. Cooke, D. A. Hewitt, D. A. Stone, and J. E. Green, “Magnetic tomography for lead acid batteries,” *J. Energy Storage*, vol. 12, pp. 1–10, Aug. 2017, doi: 10.1016/j.est.2017.03.014.

[23] “Faraday’s Law.” Accessed: May 05, 2024. [Online]. Available: https://farside.ph.utexas.edu/teaching/316/lectures/node85.html

[24] M. Cavaliere, O. McVeigh, H. A. Jaeger, S. Hinds, K. O’Donoghue, and P. Cantillon-Murphy, “Inductive Sensor Design for Electromagnetic Tracking in Image Guided Interventions,” *IEEE Sens. J.*, vol. 20, no. 15, pp. 8623–8630, Aug. 2020, doi: 10.1109/JSEN.2020.2984323.

[25] “Mutual Inductance - an overview | ScienceDirect Topics.” Accessed: May 07, 2024. [Online]. Available: https://www.sciencedirect.com/topics/engineering/mutual-inductance

[26] A. Khatun, “Direct and Non-Invasive Monitoring of Battery Internal State Via Novel GMI-IDT Magnetic Sensor”.

[27] N. V. Mushnikov, “Chapter 2 - Basics of magnetism and magnetic materials,” in *Magnetic Materials and Technologies for Medical Applications*, A. M. Tishin, Ed., in Woodhead Publishing Series in Electronic and Optical Materials. , Woodhead Publishing, 2022, pp. 23–55. doi: 10.1016/B978-0-12-822532-5.00010-8.

[28] N. Goel, A. Babuta, A. Kumar, and S. Ganguli, “Hall effect instruments, evolution, implications, and future prospects,” *Rev. Sci. Instrum.*, vol. 91, no. 7, p. 071502, Jul. 2020, doi: 10.1063/5.0009647.

[29] X. Shen, Y. Teng, and X. Hu, “Design of a Low-Cost Small-Size Fluxgate Sensor,” *Sensors*, vol. 21, no. 19, Art. no. 19, Jan. 2021, doi: 10.3390/s21196598.

[30] J. E. Davies, J. D. Watts, J. Novotny, D. Huang, and P. G. Eames, “Magnetoresistive sensor detectivity: A comparative analysis,” *Appl. Phys. Lett.*, vol. 118, no. 6, p. 062401, Feb. 2021, doi: 10.1063/5.0038187.

[31] “Highly Sensitive Magnetic Sensor Based on Anisotropic Magnetoresistance Effect | IEEE Journals & Magazine | IEEE Xplore.” Accessed: May 05, 2024. [Online]. Available: https://ieeexplore.ieee.org/abstract/document/8400533

[32] C. Reig and M.-D. Cubells-Beltrán, “Giant Magnetoresistance (GMR) Magnetometers,” in *High Sensitivity Magnetometers*, A. Grosz, M. J. Haji-Sheikh, and S. C. Mukhopadhyay, Eds., Cham: Springer International Publishing, 2017, pp. 225–252. doi: 10.1007/978-3-319-34070-8_8.

[33] C. Mușuroi, M. Oproiu, M. Volmer, and I. Firastrau, “High Sensitivity Differential Giant Magnetoresistance (GMR) Based Sensor for Non-Contacting DC/AC Current Measurement,” *Sensors*, vol. 20, no. 1, Art. no. 1, Jan. 2020, doi: 10.3390/s20010323.

[34] Z. Zhou, K. Zhang, and Q. Leng, “Tunneling Magnetoresistance (TMR) Materials and Devices for Magnetic Sensors,” in *Spintronics*, John Wiley & Sons, Ltd, 2022, pp. 51–92. doi: 10.1002/9781119698968.ch3.

References

[35] Z. Jin *et al.*, "Highly-sensitive magnetic sensor for detecting magnetic nanoparticles based on magnetic tunnel junctions at a low static field," *AIP Adv.*, vol. 11, no. 1, p. 015046, Jan. 2021, doi: 10.1063/9.0000189.

[36] "(4) (PDF) Detection of Small Magnetic Fields Using Serial Magnetic Tunnel Junctions with Various Geometrical Characteristics." Accessed: May 08, 2024. [Online]. Available: https://www.researchgate.net/publication/346127176_Detection_of_Small_Magnetic_Fields_Using_Serial_Magnetic_Tunnel_Junctions_with_Various_Geometrical_Characteristics

[37] J. Chen, J. Li, and L. Xu, "Highly Integrated MEMS Magnetic Sensor Based on GMI Effect of Amorphous Wire," *Micromachines*, vol. 10, no. 4, p. 237, Apr. 2019, doi: 10.3390/mi10040237.

[38] Y. Wang, *Introduction to SQUID Sensors for Electronics Engineers*. 2023. doi: 10.48550/arXiv.2310.00573.

[39] M. A. Khan, J. Sun, B. Li, A. Przybysz, and J. Kosel, "Magnetic sensors-A review and recent technologies," *Eng. Res. Express*, vol. 3, no. 2, p. 022005, Jun. 2021, doi: 10.1088/2631-8695/ac0838.

[40] N. Khare, P. Singh, and J. Vassiliou, "Method and system for magnetic field probing for sealed-acid battery diagnosis," US9184611B2, Nov. 10, 2015 Accessed: Mar. 12, 2024. [Online]. Available: https://patents.google.com/patent/US9184611B2/en

[41] R. Chen *et al.*, "Power Batteries Health Monitoring: A Magnetic Imaging Method Based on Magnetoelectric Sensors," *Materials*, vol. 15, no. 5, p. 1980, Mar. 2022, doi: 10.3390/ma15051980.

[42] M. Mohammadi, E. V. Silletta, A. J. Ilott, and A. Jerschow, "Diagnosing current distributions in batteries with magnetic resonance imaging," *J. Magn. Reson.*, vol. 309, p. 106601, Dec. 2019, doi: 10.1016/j.jmr.2019.106601.

[43] "Applied Sciences | Free Full-Text | Determination of SoH of Lead-Acid Batteries by Electrochemical Impedance Spectroscopy." Accessed: May 05, 2024. [Online]. Available: https://www.mdpi.com/2076-3417/8/6/873

[44] Y. Guo, "A sensor of sulfuric acid specific gravity for lead-acid batteries," *Sens. Actuators B Chem.*, vol. 105, no. 2, pp. 194–198, Mar. 2005, doi: 10.1016/j.snb.2004.05.061.

[45] A. M. Cao-Paz *et al.*, "A Multi-Point Sensor Based on Optical Fiber for the Measurement of Electrolyte Density in Lead-Acid Batteries," *Sensors*, vol. 10, no. 4, Art. no. 4, Apr. 2010, doi: 10.3390/s100402587.

[46] "State-of-charge determination of lead-acid batteries using wire-wound coils - ScienceDirect." Accessed: Apr. 29, 2024. [Online]. Available: https://www.sciencedirect.com/science/article/pii/S0378775305008591

[47] J. A. Tinnemeyer, "31-4: Diamagnetic Measurements in Lead Acid Batteries to Estimate State of Charge".

[48] V. Refko, E. Shembel, and V. Khandetskyy, "Apparatus and method for determining service life of electrochemical energy sources using combined ultrasonic and electromagnetic testing," US20080028860A1, Feb. 07, 2008 Accessed: Apr. 29, 2024. [Online]. Available: https://patents.google.com/patent/US20080028860A1/en

[49] B. J. Koch, "Battery magnetic state of charge sensor control algorithm," US9461485B2, Oct. 04, 2016 Accessed: Apr. 28, 2024. [Online]. Available: https://patents.google.com/patent/US9461485B2/en

References

[50] J. E. Green, D. A. Stone, M. P. Foster, and A. Tennant, "Spatially Resolved Measurements of Magnetic Fields Applied to Current Distribution Problems in Batteries," *IEEE Trans. Instrum. Meas.*, vol. 64, no. 4, pp. 951–958, Apr. 2015, doi: 10.1109/TIM.2014.2362432.

[51] J. A. Tinnemeyer, "Methods and apparatus for battery testing," US20130093428A1, Apr. 18, 2013 Accessed: Apr. 29, 2024. [Online]. Available: https://patents.google.com/patent/US20130093428/en

[52] K. Yanamandra, D. Pinisetty, A. Daoud, and N. Gupta, "Recycling of Li-Ion and Lead Acid Batteries: A Review," *J. Indian Inst. Sci.*, vol. 102, no. 1, pp. 281–295, Jan. 2022, doi: 10.1007/s41745-021-00269-7.

[50] J. E. Green, D. A. Stone, M. P. Foster, and A. Tennant, "Spatially Resolved Measurements of Magnetic Fields Applied to Current Distribution Problems in Batteries," *IEEE Trans. Instrum. Meas.*, vol. 64, no. 4, pp. 951–958, Apr. 2015, doi: 10.1109/TIM.2014.2362432.

[51] J. A. Tinnemeyer, "Methods and apparatus for battery testing," US20130093428A1, Apr. 18, 2013 Accessed: Apr. 29, 2024. [Online]. Available: https://patents.google.com/patent/US20130093428/en

[52] K. Yanamandra, D. Pinisetty, A. Daoud, and N. Gupta, "Recycling of Li-Ion and Lead Acid Batteries: A Review," *J. Indian Inst. Sci.*, vol. 102, no. 1, pp. 281–295, Jan. 2022, doi: 10.1007/s41745-021-00269-7.

[53] S. Dhundhara, Y. P. Verma, and A. Williams, "Techno-economic analysis of the lithium-ion and lead-acid battery in microgrid systems," *Energy Convers. Manag.*, vol. 177, pp. 122–142, Dec. 2018, doi: 10.1016/j.enconman.2018.09.030.

[54] M. Kwiecien *et al.*, "Variation of Impedance in Lead-Acid Batteries in the Presence of Acid Stratification," *Appl. Sci.*, vol. 8, no. 7, Art. no. 7, Jul. 2018, doi: 10.3390/app8071018.

[55] U. Sydow, M. Buhlert, E.-C. Hass, and P. Plath, "Spatial Inhomogeneity in Lead-Acid Batteries," 2004, pp. 593–605. doi: 10.1002/3527602585.ch33.

Appendix

Magnetic Susceptibility Introduction

VILLANOVA UNIVERSITY

Introduction and Background

- **Magnetic susceptibility (χ_m)** indicates the ability of a material to be magnetized in response to an applied magnetic field.
- It provides a measure of how a material will react when placed in a magnetic field.

It is calculated as the ratio of the magnetization (M) of the material to the applied magnetic field strength (H)

$$\chi_m = \frac{M}{H}$$

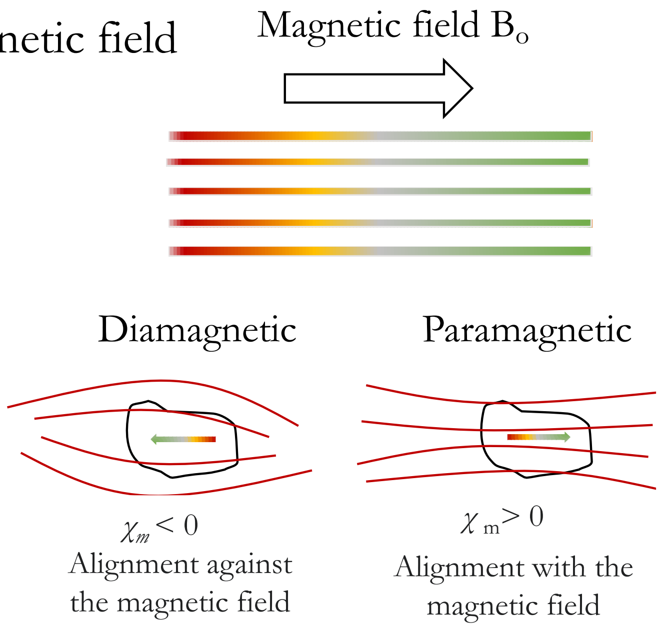

- Depending on the atomic composition of a substance, it can have a diamagnetic or paramagnetic response.

Air Core Solenoid Magnetic Field

Introduction and Background

The magnetic field strength, B , inside the center of a solenoid is calculated using the equation:

$$L = \frac{N^2 \mu A}{I}$$

$$\mu = \mu_I \mu_0$$

$$\mathrm{B} = 7.074 \text{ x}10^{-6} \text{ T}$$

Where,

L= Inductance of coil (H)
N=Number of turns in the coil
μ=Permeability of core material
μ_I=Relative permeability, dimensionless (μ0=1 for air)
μ_0 =1.26x10^{-6} T m/At permeability of free space
A=Area of coil in square meters=πr^2 (See figure 6)
l=Average length of coil in meters

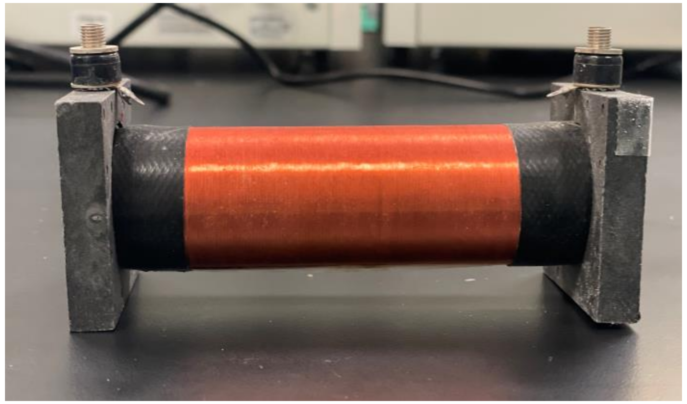

Fig. 8 Air Core Solenoid Inductor

A changing magnetic field, induces an electric field, which results in an induced voltage response

Magnetic Field Technique Concepts

The magnetic field resulting from a typical lead acid cell is given by the Biot-Savart law, which measures the magnetic field generated by an electric current.

The equation is as follows:

$$B_m = \frac{\mu_0 I}{2\pi r}$$

where,

B_m Is magnitude of magnetic field measured by a sensor
μ_0 Is the permeability of free space
I Is the current
r Is the perpendicular distance from the sensor to the coil